ACADEMIC PRESS

Available online at www.sciencedirect.com
SCIENCE DIRECT®

Journal of Catalysis 216 (2003) 246–256

JOURNAL OF CATALYSIS

www.elsevier.com/locate/jcat

Local manipulation of catalytic surface reactivity

J. Wolff,[a] A.G. Papathanasiou,[a] H.H. Rotermund,[a,*] G. Ertl,[a] X. Li,[b] and I.G. Kevrekidis [b]

[a] *Fritz-Haber-Institut der Max-Planck-Gesellschaft, Faradayweg 4-6, Berlin D 14195, Germany*
[b] *Department of Chemical Engineering, Princeton University E-Quad, Olden St, Princeton, NJ 08544, USA*

Received 15 August 2002; revised 6 November 2002; accepted 19 November 2002

Abstract

Utilizing a focused laser beam manipulated through computer-controlled mirrors, and capable of "writing" spatiotemporal temperature fields on a surface, we explore here the fundamental impact of localized spatiotemporal perturbations on a simple reaction–diffusion system. Our two-dimensional model system is the low-pressure catalytic oxidation of CO on Pt(110), a reaction exhibiting well-understood spatiotemporal patterns. In the simplest case the laser spot causes the ignition of a reaction wave by a single critical "kick" at a selected surface location. The cooperativeness between two local *subcritical* perturbations separated in time and/or space is then explored. A temperature heterogeneity moving along a line may ignite waves along its path, or can drag preexisting pulses. In the oscillatory region we find localized beat patterns when the laser spot moves along a circle. The ratio between the underlying natural oscillation frequency and the forcing (circle-writing) frequency is important here. Finally we demonstrate how pulses, the basic building blocks of chemical patterns, can be modified, guided, and erased and how the overall reaction rate can be increased through localized actuation. Computational studies supplement and rationalize the experimental findings.

Keywords: Co oxidation; Pattern formation; Pt(110); Addressable catalyst; Structured perturbation

1. Introduction

Controlling the course of chemical reactions is a vital component of chemical process industries for productivity and safety as well as environmental reasons (e.g., [1]). Conceptually different approaches at various levels of complexity are used to achieve this control. For homogeneously catalyzed reactions global feedback is often the method of choice [2]. Heterogeneously catalyzed reactions allow a more direct approach, especially with model systems in which the educts are delivered via the gas phase and a single crystal is used as the catalytic surface. Since the surface of the catalyst is two-dimensional, it is in some cases possible through resolved spectroscopic/optical methods to gain locally resolved information and, at the same time, "talk back" to the local dynamics of the reaction. Of course, real world heterogeneous catalysis occurs on high-surface-area materials, which are not easily accessible for locally resolved sensing and actuation.

In the case of single-crystal catalysts, spatially resolved actuation can be implemented by manipulating laser light through computerized optics. Reaction conditions are locally altered through differential heating, thus creating spatiotemporally addressable catalytic surfaces [3]. When the reactions under investigation exhibit pattern formation, this spatiotemporal addressing of surface activity is a powerful tool in altering open-loop system behavior. In our addressable catalyst work we have demonstrated how catalytic dynamics could be affected through this approach. Pulses and fronts, the basic building blocks of chemical patterns, could be formed, modified, guided, and erased through localized space/time actuation [3]. As the ultimate limit, even reaction steps between individual surface species may be controlled by means of scanning tunneling microscopy [4,5].

In more recent work we demonstrated that non-steady-state, spatiotemporally programmable operation can be used to systematically improve the rate of a relatively simple catalytic reaction [6]. As sensing and actuation become increasingly resolved in space and time, complicated spatiotemporal operating policies become accessible. The ultimate dream of optimal operation based on "finely resolved" actuation and sensing is still precisely this, a dream, and the mathematics of such an enterprise are at least as complex

* Corresponding author.
E-mail address: rotermun@fhi-berlin.mpg.de (H.H. Rotermund).

0021-9517/03/$ – see front matter
doi:10.1016/S0021-9517(02)00131-8

as the technology of the sensing and actuation. Current efforts focus on exploring the "simplest nontrivial" open- and closed-loop spatiotemporal policies.

This paper explores the manipulation of the reaction dynamics of CO oxidation on a Pt(110) single-crystal surface using a focused laser system capable of "writing" spatiotemporal temperature heterogeneity patterns on the metal single-crystal catalyst. We start by investigating the simplest operation: the ignition of pulses or fronts by introducing sudden local temperature jumps within our viewing field. We then progress to moving temperature heterogeneities, and study the creation as well as the dragging of pulses or fronts. We conclude with experiments demonstrating direct, deliberate interactions with the shape of pulses and with the overall reaction rate. While many of these results—both in experiments and in modeling—are new, we have also included, for completeness, results obtained over the past two years with appropriate references. Throughout the paper we include computational results supporting and rationalizing the experimental observations.

2. Experimental setup

Experiments were performed in an ultra-high-vacuum (UHV) chamber, equipped with a low-energy electron diffraction (LEED) system, Ar-ion sputtering, and sample heating (from the back side) via a halogen lamp. A differentially pumped quadrupole mass spectrometer was fitted to the chamber. The 10-mm diameter Pt(110) single-crystal sample was prepared by repeated cycles of Ar^+ sputtering and O_2 treatment at 570 K and subsequent annealing up to 1000 K. Gas supplies for CO and O_2 were automated and stabilized, allowing controlled settings of the partial pressures of the reactants within the UHV chamber. Adsorbate concentration patterns on the surface of the sample were imaged using ellipsomicroscopy for surface imaging (EMSI) [7]. The reaction proceeds via $O_{ad} + CO_{ad} \rightarrow CO_2$, whereby, under the experimental conditions chosen, dark areas in the images reflect enhanced concentrations of adsorbed oxygen atoms, while on the brighter areas the adsorbed CO dominates.

To achieve local heating of the surface, the light of an Ar-ion laser was focused onto a spot of diameter about 50 μm. Typical maximum temperature rises, at the center of the heating spot, were on the order of 10 K for 1 W laser power. The initial local temperature rise occurs within 5 ms. The temperature profile in general depends on the thickness of the sample and the duration of irradiation at one position. For our experiments the size of the temperature inhomogeneity closely resembles the diameter of the laser spot on the sample, as evidenced by infrared imaging. Computer-controlled galvanometer mirrors allow the positioning of the focused laser beam within 1 ms and a spatial precision of about 4 μm at any point within the viewing field (1.6×1.3 mm^2) of EMSI. During all experiments reported here, the laser spot was kept permanently on the sample, at the edge or just outside of the viewing field of EMSI, in order to ensure a constant average sample temperature.

3. Modeling

Many isothermal catalytic surface reactions have the potential for exhibiting dynamic instabilities, including bistability, excitability, and oscillatory behavior. Surface reactions usually proceed via the Langmuir–Hinshelwood (L–H) mechanism; i.e., all reactants have to adsorb onto the surface before reacting. Different site requirements for the adsorbing gases suffice to cause bistable behavior in some parameter regimes [8]. For CO oxidation, CO requires just one adsorption site, whereas O_2 adsorbs dissociatively, needing at least two adjacent adsorption sites. The bistability observed in CO oxidation can thus be directly attributed to its L–H mechanism. Oscillatory behavior or excitability, however, requires more than just different adsorption sites to occur. An additional nonlinearity (feedback loop) must exist. Possible mechanistic origins of this feedback are compiled in [9] and an overview of different models describing surface reactions is given in [10].

The mechanistic reaction–diffusion model capable of predicting the oscillatory behavior of CO oxidation on Pt(110) is based on a surface phase transition, due to CO adsorption [11]. The clean Pt(110) surface is reconstructed in a missing row state, exhibiting a 1×2 LEED pattern. Adsorption of 0.5 ML of CO will lift the reconstruction completely [12,13], and a bulk-like surface structure showing a 1×1 LEED pattern is established. Between 0.2 and 0.5 ML CO coverage, the fraction of the 1×1 surface increases monotonically. The fact that oxygen has a 50% higher sticking probability on the unreconstructed (as compared to the reconstructed 1×2) surface phase provides the required additional feedback loop [14,15]. If the partial pressures for the reactants are chosen so that CO adsorbs beyond a certain threshold onto the reconstructed surface, the resulting lifting of this reconstruction will favor oxygen adsorption accompanied by reactive consumption of the CO. This establishes, under appropriate conditions, an oscillating cycle. The reconstruction model [11] is described below in more detail. The control parameters are the partial pressures of CO, O_2, and the crystal temperature T, which enters via the rate constants k_2 (desorption), k_3 (reaction), and k_5 (surface phase transition) through Arrhenius activation: $k_i = (k^0)_i \exp(-E/RT)$. The model is

$$\begin{aligned}
\frac{\partial u}{\partial t} &= k_u s_u p_{CO}\left[1 - \left(\frac{u}{u_s}\right)^3\right] - k_2 u - k_3 u v + \nabla \cdot (D_u \nabla u),\\
\frac{\partial v}{\partial t} &= k_v p_{O_2}\big[w s_{v1} + s_{v2}(1-w)\big]\left(1 - \frac{u}{u_s} - \frac{v}{v_s}\right)^2 - k_3 u v,\\
\frac{\partial w}{\partial t} &= k_5\big(f(u) - w\big), \qquad (1)
\end{aligned}$$

where u and v denote the surface coverage by CO and O, respectively, and w is the fraction of the surface area in the

1×1 phase. The function $f(u)$ in the equation for w is an experimental fit to the rate of change of the surface structure and takes the following form for a Pt(110) surface:

$$f(u) = \begin{cases} 0, & u \leqslant 0.2, \\ -\frac{1}{0.0135}\left(u^3 - 1.05u^2 + 0.3u - 0.026\right), & \\ \quad 0.2 < u < 0.5, & \\ 1, & u \geqslant 0.5. \end{cases}$$

Note that in the equation for the oxygen coverage v no desorption or diffusion term appears, since at moderate temperatures (below 550 K) the binding energy for single O atoms on Pt(110) is too high to allow significant diffusion or desorption.

So far the temperature has been treated as one of the control parameters, uniformly constant in space and time. Since we will use a local temperature field to affect the reaction, we have to consider its shape. The heat balance on the crystal surface including heat conduction, radiation, and heating by the laser dictates the temperature profile. The heat generated from the reaction at these low pressures can be estimated to be about 1 mW and can be therefore safely neglected. Since the diffusivity of heat ($\sim 10^{-1}$ cm^2/s) is much larger than that of the adsorbed carbon monoxide ($\sim 10^{-8}$ cm^2/s) under typical experimental conditions, the temperature field response time (milliseconds) is fast compared to process characteristic times (seconds). For that reason we assume that a localized, "bump-shaped" temperature field $T(x - x_0)$ is instantaneously switched "on" and "off" by moving the laser spot to and from the point of interest x_0. For our qualitative modeling, single spot simulations were radially symmetric, while two-spot simulations were one-dimensional in space. The same temperature profile was used in both. Qualitatively similar results were also obtained using Gaussian temperature profiles.

4. Results and discussion

Our work focuses on the application of systematically chosen spatiotemporal forcing functions to a simple chemical reaction. We view those forcing functions as "structured perturbations" in space and time, with the potential for implementation of "designer noise" and experimental realization of stochastic partial differential equations (SPDEs) in a later study. The simplest structured perturbation is localized in space as well as in time. It may be realized by focusing the laser beam (heating) at *a single* point (at a "pixel") for a specified time-interval Δt. The critical time $\Delta t = t_{\text{crit}}$ corresponds to the minimum excitation needed to ignite the system. At the next level of structure we still heat *one* point in space, but now at more than one instant in time. This permits the study of cooperative effects between various subcritical perturbations by varying the duration of laser shots and the time interval between them. The next step swaps time with space: we try to ignite pulses at two locations simultaneously. Experimentally this would be possible by using a beam splitter and then varying the distance between the two heating points. Due to local differences of reflectivity and limitations of optics, however, no completely symmetric two-point experiments can easily be performed in our system. For this case, we confine ourselves to simulations. We did study experimentally the cooperative effects between subcritical perturbations at one point in space followed by perturbations at a *different* point in space. If we let the spatial distance between successive laser kicks decrease and at the same time let the duration of each successive kick go to zero, we pass to the next complexity level: a heating curve in space–time. For the simplest such curve, the laser spot moves at constant speed on a straight line along the surface. We will also show experiments for curved laser paths: the simplest one is a circle drawn at constant angular velocity. We will finish with a few examples of more complex curves, a small preview of the many avenues open for exploration.

In our first study, the laser spot was initially moved from the "waiting" position to the point of interest for a time interval t_1. Then, depending on the type of experiment, it was either directed to a second spot for time t_2, or back to its "waiting" position for a delay time t_{d}. From the waiting position it either revisited the same first spot for a time t_2 or moved to a second spot for a time t_2. For each series of trials below, the CO partial pressure was kept constant. At 10 s before the first laser movement, oxygen partial pressure was raised suddenly from below 10^{-7} mbar to its default value of 3×10^{-4} mbar.

A sequence of images from a single-kick experiment at a point are shown in Fig. 1. In the beginning the laser spot sits in its waiting position outside the image and far enough away from the point of interest so that what happens in the waiting position does not affect the kick experiment. At 10 s after oxygen is let into the chamber, the laser spot jumps to the measurement point ($t = 0$ s) and stays at this position, indicated with an arrow in frame # 1, for $t_{\text{crit}} = 90$ ms. Any briefer visit of the laser spot at this point would be *subcritical*, and no reaction wave would be initiated. After the laser spot has returned to the waiting position outside the image, within a second, an O island can be seen to nucleate and grow at the measurement spot. t_{crit} depends strongly upon temperature and reactant partial pressures. Fig. 2 illustrates this t_{crit} dependency on the partial pressure of CO (p_{CO}) for a constant partial pressure of $p_{\text{O}_2} = 3 \times 10^{-4}$ mbar. The experimental "noise" is estimated to be about ± 3 ms.

After determining the critical irradiation time for single-visit ignition (t_{crit}), we studied combinations of two (subcritical) laser shots (t_1 and t_2) at the same point in space, separated by a delay time t_{d} varying between 0 and 150 ms at the waiting position. All results are scaled with the appropriate t_{crit}. The distance (in space and time) of these combined subcritical shots, along with the laser intensity, parameterizes our family of deterministic perturbations. In Fig. 3a we present experimental results for critical combinations of two subcritical kicks for three time delays (50, 100, and 150 ms). The diagonal represents "perfect memory" of the first kick.

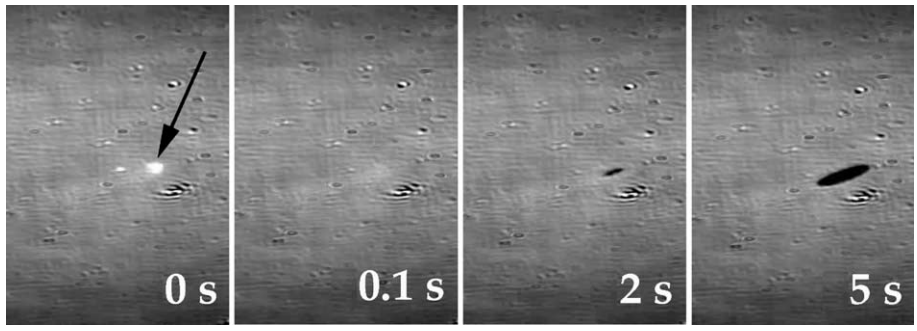

Fig. 1. A sequence of snapshots showing a successful single-spot ignition experiment. 10 s before the start of the experiment oxygen partial pressure was raised from below 10^{-7} mbar to 3×10^{-4} mbar. The critical laser shot duration was 90 ms. The laser spot position during the shot is marked by the dark arrow in the first frame. The pulse develops about 1 s after the laser has left the heating location. Experimental conditions: $p_{O_2} = 3 \times 10^{-4}$ mbar, $p_{CO} = 5.3 \times 10^{-5}$ mbar, $T = 473$ K, laser power $L_p = 2$ W, viewing area 0.8×1.1 mm^2.

For small time delays the initial kick seems to be still well remembered, while with increasing delays this memory fades more and more. Simulations presented in Fig. 3b show comparable trends. A set of data at decreased CO partial pressure is included in the simulations, showing slower memory loss. This can be rationalized through the slower readsorption of CO from the gas phase, slowing down the "healing" of the first shot.

Similar cooperative effects can be achieved by varying the spatial distance between two successive laser shots. Fig. 4a displays the necessary duration of the second shot versus the duration of the first shot (each normalized by the single critical shot duration). The separate curves are measured by changing systematically the distance of the two shot centers in space. Obviously, the further apart the two points are, the less cooperativeness is observed. For distances larger than 18 μm the memory effect practically vanishes. Fig. 4b explores the relative importance of space and time in the cooperative effect: keeping a fixed distance of 13 μm, we now vary the delay before kicking at the second spot. The loss of memory is now much more rapid than in single point experiments. A delay of 100 ms is enough to practically suppress cooperativeness.

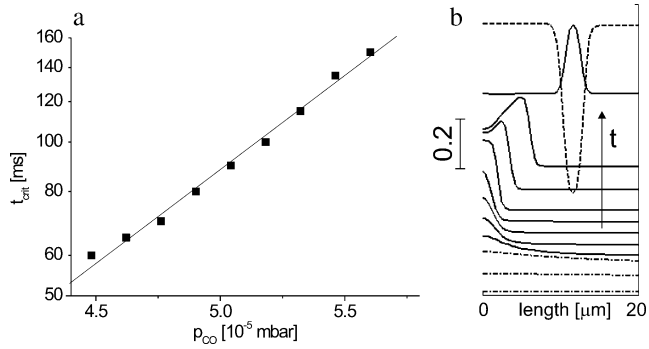

Fig. 2. (a) The critical irradiation time to ignite a pulse t_{crit} is plotted on a logarithmic scale for different partial pressures of CO. Toward smaller CO partial pressures, pulses tend to ignite at intrinsic defects on the surface, which hinders the measurement of t_{crit}. Experimental conditions: $T = 469$ K, $p_{O_2} = 3 \times 10^{-4}$ mbar, $L_p = 2$ W. (b) Computational representation of the temporal development of the oxygen coverage during a successful ignition experiment. The dash–dotted curves represent the O profile when the laser heats the surface at $x = 0$. The actual pulse develops here (as in the experiments) *after* the heating of the spot has stopped (solid curves). The dashed curve shows the CO coverage that corresponds to the last solid O curve: the pulse is now completely developed. Computational parameters: $T = 535.5$ K, $p_{CO} = 4.95 \times 10^{-5}$ mbar, $p_{O_2} = 2 \times 10^{-4}$ mbar, heating time 550 ms. The maximum temperature rise in the middle is 3.5 K.

As one might expect, if the first hit was close to critical, it is the first point that "fires" assisted by the second subcritical shot. If the first hit was strongly subcritical, one expects (and sees) the second point to "fire" upon heating. For a single set of conditions (a particular combination of t_1 and t_2) we observed both points firing simultaneously. This transition between first and second point firing for a special set of conditions was also observed computationally. Another computational observation—when the two points were relatively close—was firing from the middle region between them. Three sets of simulations along these lines are displayed in Fig. 5. Fig. 5a shows the second spot firing just after the second point on the surface has been heated by the laser. The lower three curves (dash–dotted) depict the change of oxygen coverage during the first hit (at $x = 0$ μm); the next four lines (dashed) show the changes during the subsequent second hit (at $x = 50$ μm). All following curves (solid) show the development after the heating is completed. Clearly the first solid curve indicates the initiation of the pulse at $x = 50$ μm (the "second" point). Figs. 5b and 5c show simulations for the two other observed cases: Fig. 5b analyzes the ignition of a single pulse in the middle region between the two spots (at $x = 0$ μm and 40 μm), while Fig. 5c places the kicks 50 μm apart, resulting in both points firing simultaneously.

In the bistable regime the laser shots initiate fronts rather than pulses under similar conditions. Experimentally, elliptical oxygen islands are initiated, and finally "switch" the surface from the CO-poisoned, unreactive state to the reactive one. We have studied experimentally the cooperativeness of subcritical shots in initiating fronts [16], and explored computationally the cooperativeness of two simultaneous in time, but separated in space, shots in this bistable regime also.

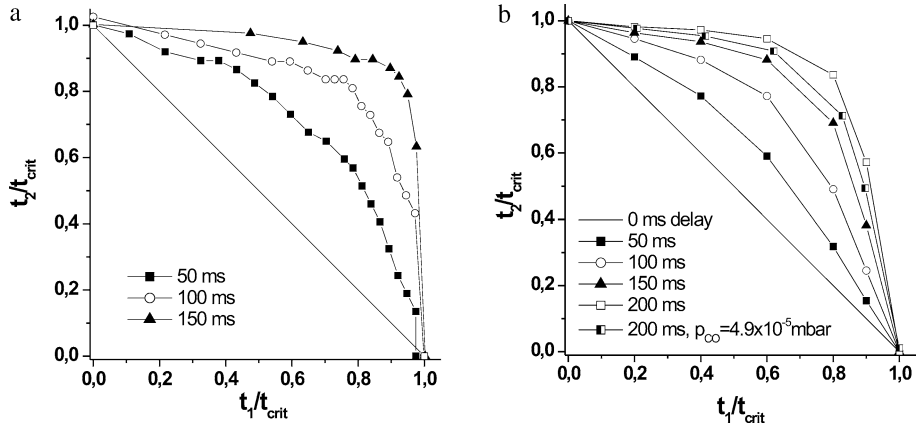

Fig. 3. (a) The critical second-kick duration t_2 (normalized by the single-kick critical time t_{crit}) required to ignite a pulse, as a function of the duration of the first subcritical kick, t_1, is plotted for three delay intervals between kicks (during which the laser is far away from the measurement point). The longer the laser waits before revisiting the preheated spot, the more the sample has "forgotten" its first visit. Experimental conditions: $L_p = 1.2$ W, $T = 475$ K, $p_{CO} = 4.2 \times 10^{-5}$ mbar, $p_{O_2} = 3 \times 10^{-4}$ mbar. (b) Computational parameters: $T = 535.5$ K, $p_{CO} = 4.95 \times 10^{-5}$ mbar, $p_{O_2} = 1.33 \times 10^{-4}$ mbar, maximum temperature rise in the middle of the spot $\Delta T = 3.5$ K.

The cooperativeness of two single laser shots in space and time having been investigated, the next step toward higher forcing function complexity is to repeatedly hit the two points under investigation. In the following experiments the heating continuously alternated between the two points in space, always with the same duration, that is $t_1 = t_2$. There was no time delay between kicks, the distance between the points was fixed, and only the kick duration was systematically varied for each fixed distance. The results of these experiments are shown in Fig. 6, where the distance of the two spots is plotted versus t_1 normalized by t_{crit}. If we were to hit two practically overlapping spots only once, the minimum time $t_1 = t_2$ required to ignite a pulse would be 0.5 t_{crit}. By heating the two separated points over and over again, it now becomes possible to ignite the medium at even smaller $t_1 = t_2$, as the effect of the heating accumulates over time. For small values of t_1 the laser spot had to hit each of the points several times before any ignition would occur. During these experiments a pulse would emerge within the first two seconds after the start of the repetitive kicking of the points, or no wave formation could be observed at all. Due to the repetitive nature of the experiment and the slightly wider laser spot profile (ca. 80 μm) the cooperative effect could now be observed even at larger distances. For times smaller than 0.85 t_{crit} cooperativeness seems to be constant and confined to roughly a distance of one laser spot radius, similarly to the single-hit experiments presented above. However, for larger laser residence times, close to the single-shot critical time, cooperativeness was observed for larger distances, up to about twice the laser spot radius.

We now proceed to use a single spatially coherent but temporally mobile, steadily moving, temperature hetero-

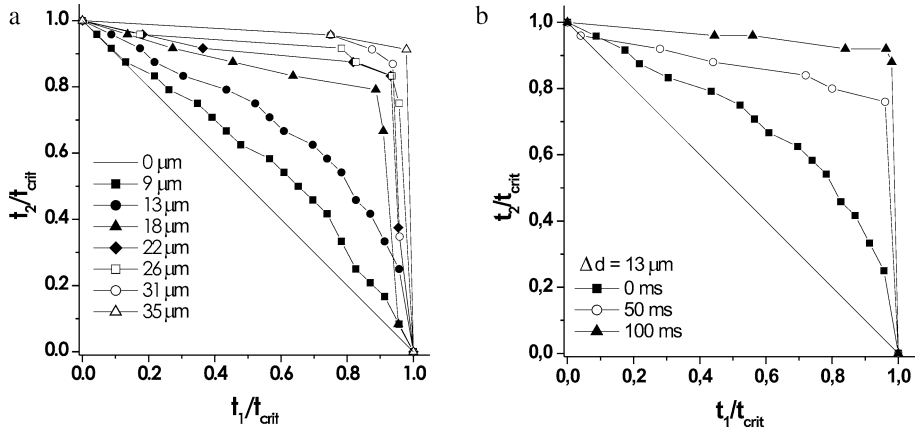

Fig. 4. (a) t_2, the critical heating time required to ignite a pulse when visiting a second point, at a distance from the original heating point about 18° off the [001] direction (slow CO diffusion), where the laser just spent time t_1. The larger the distance between the two points, the less "memory" of the first hit is retained. (b) Keeping a fixed distance (13 μm) between the two heated spots (same direction), we vary the delay time between the heating events. Cooperativeness is practically lost for waiting times exceeding about 100 ms. Experimental conditions for both: $T = 466$ K, $p_{CO} = 4.9 \times 10^{-5}$ mbar, $p_{O_2} = 3 \times 10^{-4}$ mbar, $L_p = 2$ W.

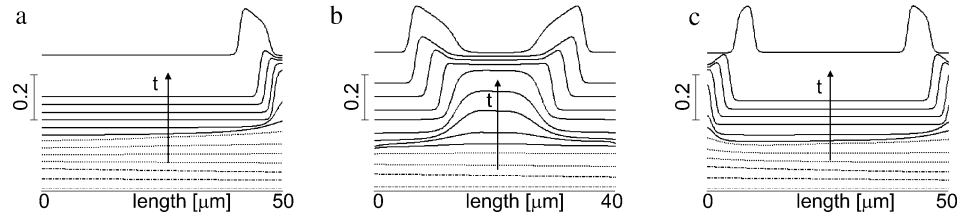

Fig. 5. Computational profiles of the development of oxygen coverages for different conditions. Dash–dotted (resp. dotted, solid) lines: initial (resp. second, post-) heating periods. (a) Development during the first laser hit at $x = 0$ μm, followed by a second laser hit at $x = 50$ μm. The solid lines show the development after both laser hits. The pulse develops towards the end of the second heating event (last dotted curve). In (b) the pulse develops between the two heated points, 40 μm apart, while in (c) two distinct pulses develop, one at each heating point. Computational parameters for all three: $T = 535.5$ K, $p_{CO} = 4.95 \times 10^{-5}$ mbar, $p_{O_2} = 2 \times 10^{-4}$ mbar, laser width 90 μm. Maximum temperature rise for (a) and (c) was 3.5 K, for (b) 5 K.

geneity. By drawing this temperature line we will, depending on the speed of the laser spot movement and the laser power, continuously generate pulses, partially generate some, or not ignite any pulses at all. A sequence of images representative of partial creation of pulses is presented in Fig. 7. In frame # 1 the laser spot rests near the lower left corner of the image and starts to create a target pattern. The spot is then moved across the surface toward the upper right corner at 0.75 mm/s and partially ignites waves along its path (frame # 2 and frame # 3). In frame # 4 the laser spot has already returned to its resting position. The "missing links" of frame # 2 and frame # 3 along the laser path have been covered with oxygen by now. At slightly higher laser speeds no oxygen waves would be visible; at slower speeds a continuous "oxygen line" would be drawn.

A systematic compilation of line experiments performed with laser powers between 1 and 4 W is presented in Fig. 8. Two transition regions are plotted: one is the transition between the continuous generation (ignition) of waves and partial generation, while in the next column the transition is between partial ignition and "no ignition." The laser spot speeds vary between 0.2 and 55 mm/s depending on laser power and which transition is investigated. The effect of anisotropy is also visible in this figure. Transition boundaries are plotted as a function of CO partial pressure

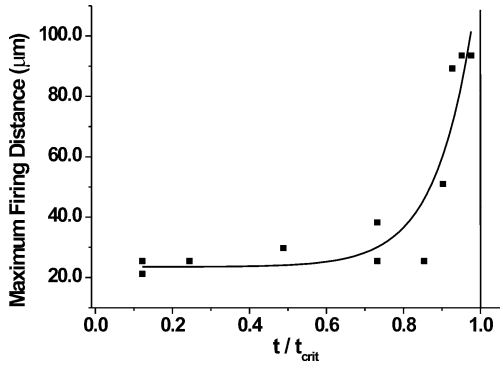

Fig. 6. Repeatedly heating two alternating points at fixed distances. The maximum distance for which a pulse is eventually generated is plotted for different residence times $t_1 = t_2$ of the laser at each point (normalized to t_{crit}). The line is an exponential fit that acts as a guide to the eye. Experimental conditions: $T = 455$ K, $p_{CO} = 4.6 \times 10^{-5}$ mbar, $L_p = 1.5$ W.

for three different laser movement directions: along the [1$\bar{1}$0] direction (corresponding to fast CO diffusion), along the [001] direction, and along an intermediate direction. Starting from the 1W results, it appears that the influence of direction for the first transition (between continuous and partial ignition) becomes more pronounced as the laser power—and with it the actual speeds of laser motion across the surface—increases. For 1W laser power the laser movement direction across the surface has no visible effect: the three curves are practically identical. Increasing the laser power causes increasingly pronounced variations. It appears that the second transition (between partial ignition and no ignition) is hardly influenced at all by anisotropy.

Instead of pulse generation by a single laser spot movement, one could try to use a laser line segment of defined length and width, and generate pulses by sweeping this line segment along the surface. Experiments of this nature are underway. Experimentally, it is easier to "approximate" such a temperature heterogeneity by combining a steady movement of the laser spot with a transverse oscillation along a short line segment. Depending on the oscillation speed of the laser spot between the edges of this segment, and its relation to the steady average transverse speed, substantially different images can result. Two sets of snapshots for slightly different cases are shown in Fig. 9.

Up to this point we have used the laser spot to ignite waves along its path. If the intensity of the laser is reduced, so that it is incapable of generating fronts or pulses,

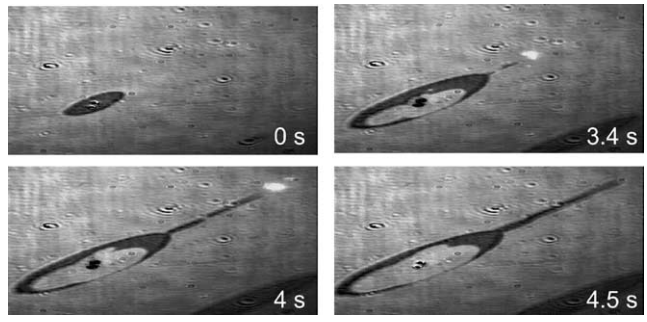

Fig. 7. Partial ignition by a moving laser spot. Image size 1.6×0.8 mm^2. Experimental conditions: $T = 493$ K, $p_{CO} = 6.4 \times 10^{-5}$ mbar, $p_{O_2} = 3.0 \times 10^{-4}$ mbar. The laser movement direction was about 10° off [1$\bar{1}$0] (corresponding to fast CO-diffusion).

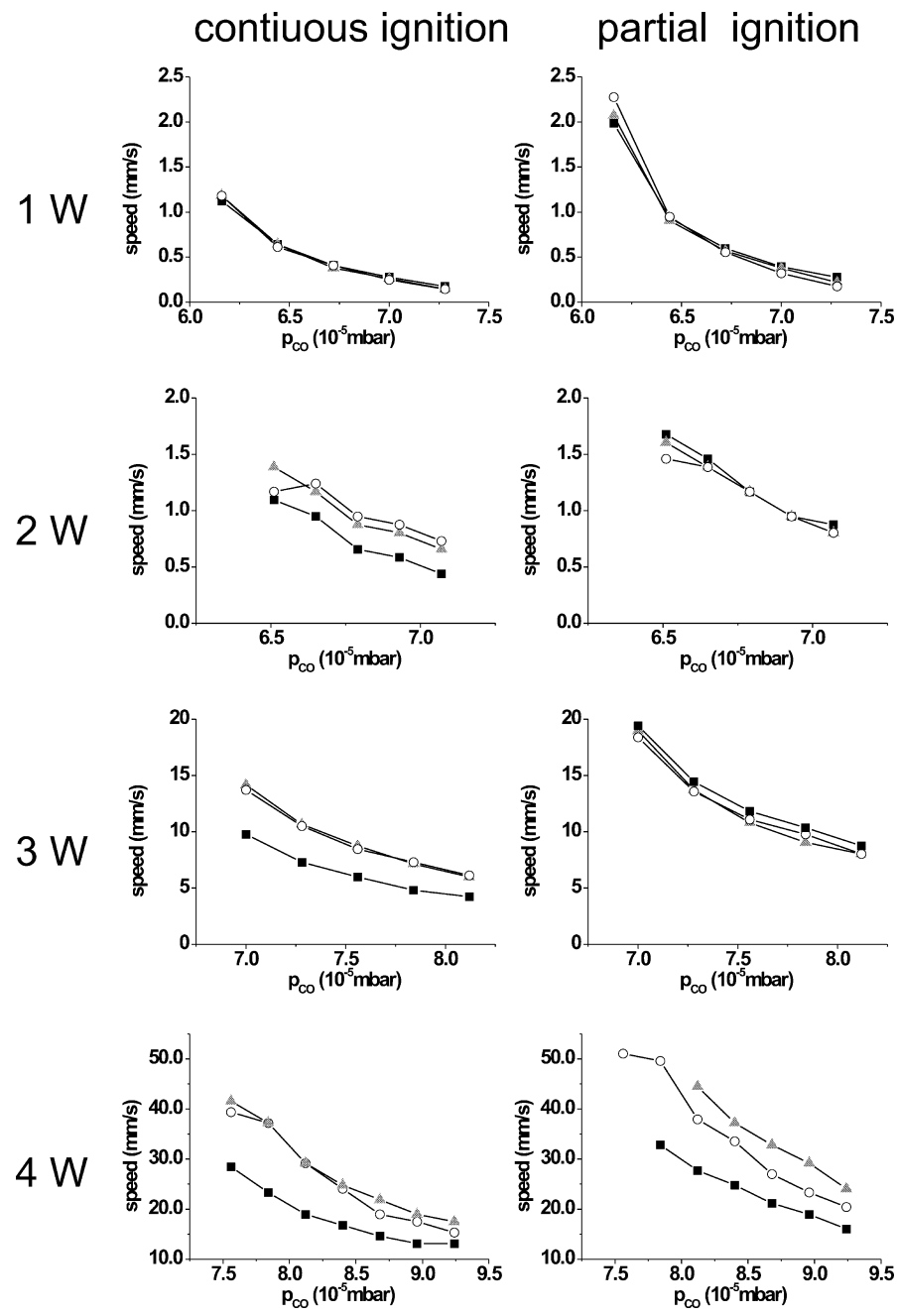

Fig. 8. The left column shows the maximum laser speed for which continuous ignition is observed for four distinct laser powers (1–4 W). For higher speeds ignition is interrupted at least at one point in space. The right column shows the partial ignition boundary: the maximum laser speed for which at at least one point on the path a pulse is ignited (again for the same four laser powers). For both columns the laser path was chosen along three directions: fast diffusion direction (open circles), slow diffusion direction (black squares) and an intermediate direction (gray triangles). Experimental conditions: $T = 495$ K, $p_{O_2} = 3 \times 10^{-4}$ mbar, p_{CO} marked on the abscissas.

a different kind of experiment can be performed. We have studied extensively this dragging of reaction waves [17]. To achieve "gentle" dragging the laser power was reduced to 1 W, and the laser was used to drag *preexisting* reaction waves that had spontaneously formed on the surface. When a steady pulse was formed, the laser spot was placed close to it, and then dragged it along a straight line with constant speed slightly higher than the natural wave speed. This is illustrated in Fig. 10, showing several pulse dragging snapshots. The black arrow indicates the position of the laser spot. As soon as a pulse appears, the spot is moved into its path. In frame # 3 the pulse reached the spot, which we then start to move at a constant speed, 79% higher than the natural pulse speed. Complete pulse dragging ensues. In a subsequent experiment, but at a laser speed 98% faster than the natural pulse speed, the dragging persists for about 10 s. Then the pulse detaches from the laser spot, and relaxes to its original shape and speed. Fig. 11 shows a

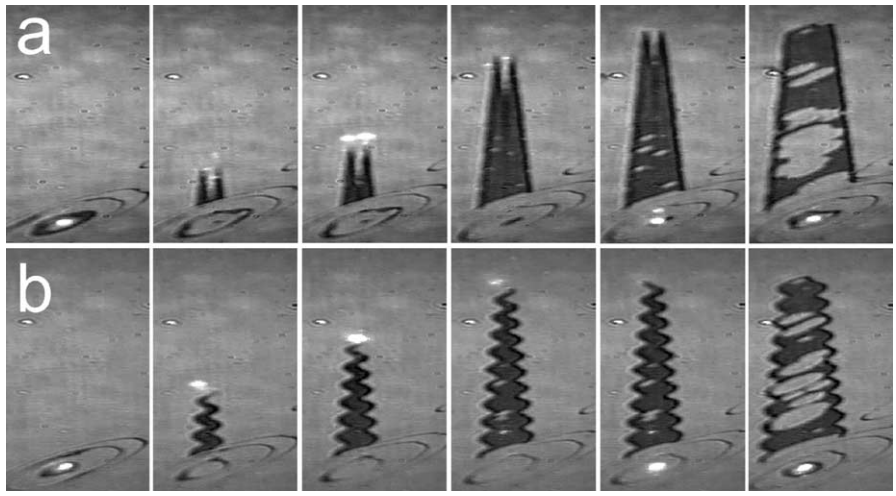

Fig. 9. Snapshots showing two experiments where the laser spot is moved back and forth between two points transversely to a steady average progression. (a) The laser moves with a speed of 15 mm/s between the two endpoints. Pulse ignition appears to occur only at the endpoints of the transverse movement. (b) The laser moves with a speed of only 1.5 mm/s. Pulse generation occurs constantly, but because the oscillatory horizontal laser speed is of the order of the vertical speed a "snake" is being drawn. Image size is 0.6×1.1 mm^2. Vertical dragging speed: 0.6 mm/s. Experimental conditions: $T = 495$ K, $p_{CO} = 7.0 \times 10^{-5}$ mbar, $p_{O_2} = 3.0 \times 10^{-4}$ mbar.

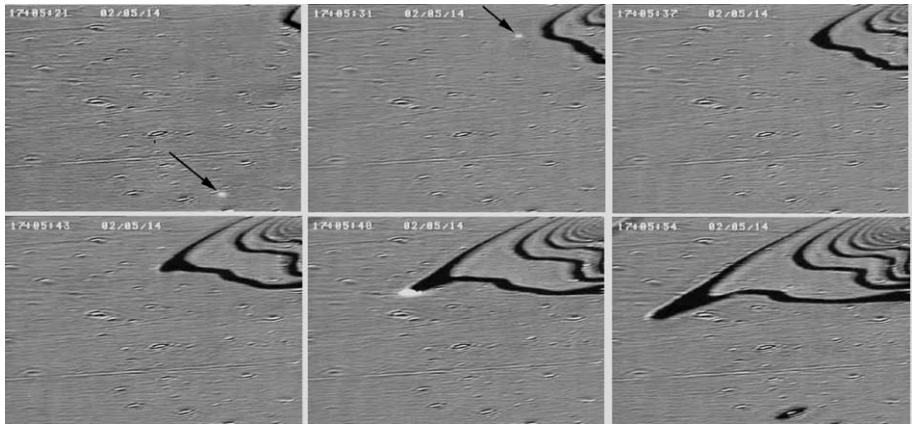

Fig. 10. Snapshots (1.6×1.1 mm^2) showing the dragging of a preexisting pulse by a "low-strength" temperature heterogeneity, incapable of igniting the medium by itself. The dragging direction was about 10° off $[1\bar{1}0]$ (corresponding to fast CO-diffusion). Experimental conditions: $T = 456$ K, $p_{CO} = 3.9 \times 10^{-5}$ mbar, $p_{O_2} = 3.0 \times 10^{-4}$ mbar.

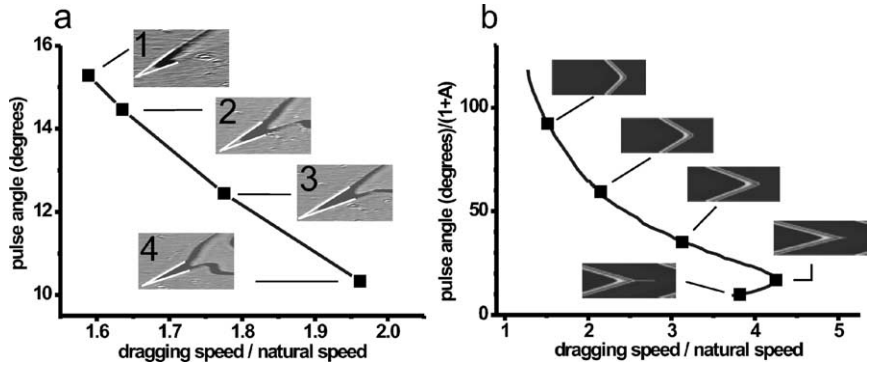

Fig. 11. Taken from [17]: Experimental (a) and computed (b) dependence of the leading angle of the dragged pulse on the dragging speed (normalized with natural pulse speed and A, the distance of laser spot and tip of pulse). Experimental conditions: $T = 456$ K, $p_{CO} = 3.9 \times 10^{-5}$ mbar, $p_{O_2} = 3.0 \times 10^{-4}$ mbar. The dragging direction was about 10° off $[1\bar{1}0]$ (corresponding to fast CO-diffusion). The angle is marked by white lines (a) in the 0.7×0.4 mm^2 insets. Computational parameters: $T = 540$ K, $p_{CO} = 4.52 \times 10^{-5}$ mbar, $p_{O_2} = 1.33 \times 10^{-4}$ mbar, and $D_{CO} = 1$ μm^2/s, 180×60 μm^2 domain; boundary conditions periodic in x and no flux in y.

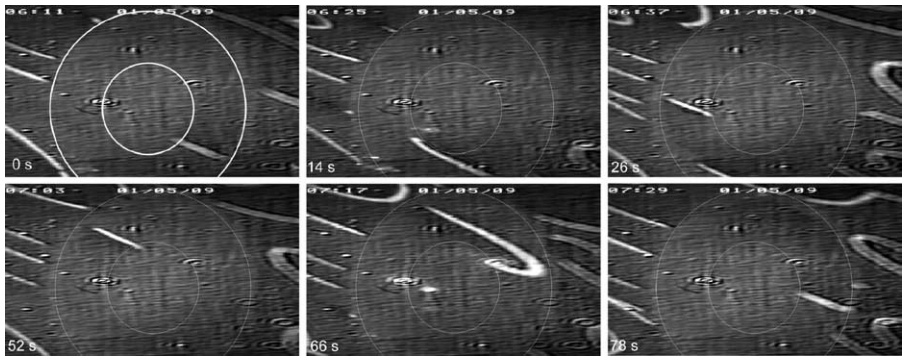

Fig. 12. The laser draws two concentric circular paths with diameters 1.1 and 0.5 mm, respectively, marked by white lines (thicker in the first image). A pulse is captured between the two circles and is forced to move around the ring. Experimental conditions: $p_{O_2} = 3 \times 10^{-4}$ mbar, $p_{CO} = 5.1 \times 10^{-5}$ mbar, $T = 479$ K (taken with permission from [3]).

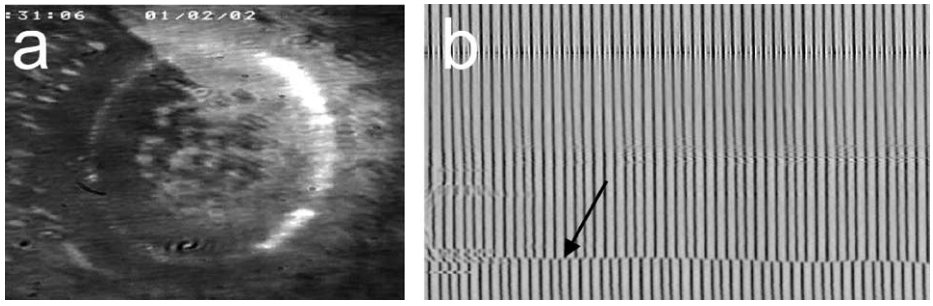

Fig. 13. (a) Snapshot that shows a phase jump (at about 11 o'clock for this particular experiment). The laser has a rotation frequency of about 3.2 Hz, while the background oscillates at about 1.8 Hz. (b) x–t plot taken just outside of and parallel to the laser path. The phase jump is clearly visible at the bottom of the x–t plot. Experimental conditions: $T = 554$ K, $p_{CO} = 1 \times 10^{-4}$ mbar, $p_{O_2} = 3 \times 10^{-4}$ mbar.

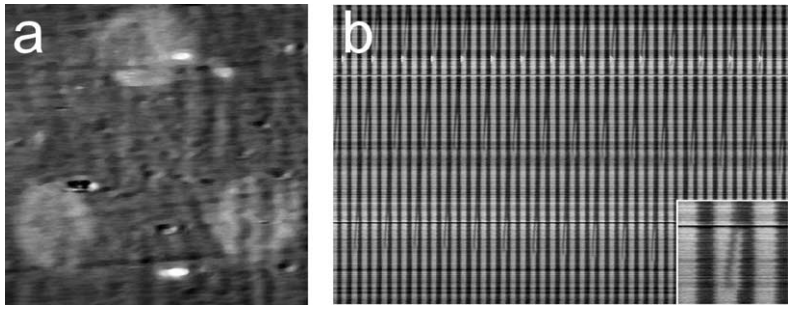

Fig. 14. (a) Three snapshots, assembled into a single image, illustrating the three-fold symmetry observed during a circle drawing laser experiment. The bright spots appear one after the other in succession. The laser draws the circle clockwise. (b) Corresponding x–t plot taken just outside, and parallel to, the laser's path in the counterclockwise direction. The inset shows an enlargement of one of the disturbances. The bright area extending into the dark region of the homogeneous oscillation corresponds to one of the bright areas in (a). Experimental conditions: $T = 516$ K, $p_{CO} = 9 \times 10^{-5}$ mbar, $p_{O_2} = 3 \times 10^{-4}$ mbar, $L_p = 3$ W.

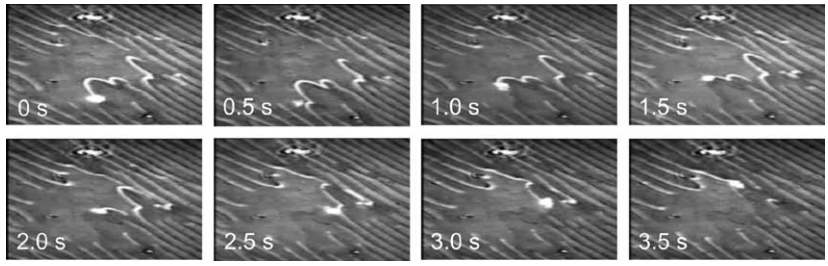

Fig. 15. A computer mouse is used to guide the laser spot on the sample surface. Through differential local heating it removes CO waves, and returns the sample at those locations to the reactive state. Experimental conditions: $p_{O_2} = 3 \times 10^{-4}$ mbar, $p_{CO} = 7 \times 10^{-5}$ mbar, $T = 505$ K. Image size: 1.7×1 mm^2.

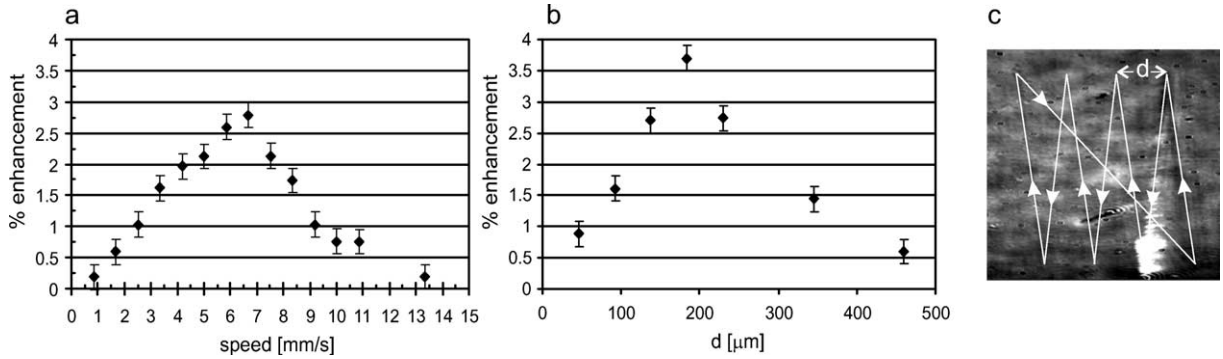

Fig. 16. CO_2 production rate enhancement versus (a) scanning speed and (b) step size d. The scanning path is depicted in (c). In (a) the step size is 150 μm; in (b) the speed is 5.5 mm/s. $p_{CO} = 10.1 \times 10^{-5}$ mbar, $p_{O_2} = 3 \times 10^{-4}$ mbar, $T = 516$ K.

compilation of these experiments and compares them with simulations. Fig. 11a shows the change of dragged pulse "cone angle" with the dragging speed. This angle varies between 15° and 10°. Higher dragging speeds, and therefore smaller angles, lead to eventual detachment and loss of the pulse. Computer-assisted modeling was used to analyze the dragging phenomenon. Fig. 11b and its insets show a bifurcation diagram with respect to the dragging/natural speed ratio. The last inset shows an unstable dragged pulse and a thin "tether" connecting its tip with the dragging heterogeneity, suggestive of pulse detachment.

We continue increasing the "forcing function complexity" by guiding the laser spot along a circle at constant angular velocity. In the excitable regime this can be used to guide pulses along a circular path by laser-drawing two concentric circles as shown in Fig. 12. All pulses external to the drawn circular corridor are kept out, while the pulse trapped inside the corridor cannot leave it. Using this technique, it is conceptually possible to "deliver" a chemical species from the area where it was created to any other part of the surface, where it might be involved in a different reaction.

Leaving the excitable regime, we now study the effect of laser heating under oscillatory conditions. Our spatiotemporal laser forcing is in the form of a single, constantly redrawn, circle. Depending on the ratio between rotation frequency and the frequency of the underlying homogeneous reaction oscillations, several distinct phenomena have been observed. Figs. 13 and 14 show representative experimental snapshots. The first example shows a phase jump occurring at about 11 o'clock. To analyze a long sequence of images (e.g., a video), profiles along a line of interest are taken from each consecutive image. They are then plotted versus time in a so-called space–time (x–t) diagram. Since the forcing is along a circle, we show our data not along straight lines cutting through this circle, but parallel to—and just outside—the circular path drawn by the laser. In this case (Fig. 13b) the x–t plot clearly shows the phase jump at a single location along the path, indicated by the black arrow. In Fig. 14 a threefold symmetry observed in another experiment is artificially displayed. Three consecutive appearances of a bright region are assembled into one image by taking corresponding slices from three individual images. The x–t plot, taken just outside and parallel to the circular path drawn by the laser, shows that the three disturbances precess slowly around the circle. The ratio of the frequency of the homogeneous background oscillation to the circle-drawing frequency was slightly below 3:1. The inset in the x–t plot shows an enlargement of one of the disturbances. A single bright area of the assembled snapshot (a) corresponds to the bright region penetrating inside the dark of the homogeneous oscillation in the inset of (b). There, the global oscillation is momentarily delayed, giving rise to the observed pattern.

Up to this point we have discussed local perturbations generated by fairly simple movements of a laser spot, along either straight lines with steady speeds, or with constant angular velocity around circles. In the last part of this paper, the laser spot velocity is no longer restricted: it can change in direction and value at the will of the experimenter. To illustrate these somewhat erratic-looking motions, Fig. 15 displays eight snapshots taken at time intervals of 0.5 s, where the laser spot is utilized by the operator via direct real-time mouse control to erase CO pulses on the surface. The goal here is to annihilate as many CO pulses as possible. All brighter areas are CO covered, and even a fast moving laser spot will erase them. Since an area covered by CO is catalytically inactive, "cleaning off" the CO will increase the reaction rate. In a straightforward experiment it has been shown that indeed the reaction rate can be increased by simply moving the laser back and forth across a mainly CO-covered surface [6]. Under constant operating conditions, the laser spot scanning path could be tuned to optimize the production rate of CO_2. This rate was directly measured with a differentially pumped quadrupole mass spectrometer. By performing a linear scanning as shown in Fig. 16c the rate enhancement is found to depend on the speed and the step size, d. The exploration of this dependence toward maximizing the CO_2 production rate revealed optimum values for scanning speed as well as for step size (see Figs. 16a, 16b).

In a Gedankenexperiment one could think about improving the selectivity of a more complicated reaction. Looking again at Fig. 15, imagine that it displays intermediate

species, say A (bright waves in the middle) and B (black and gray pulses on the sides). By erasing only A its further reaction would be suppressed and thus the selectivity affected.

5. Conclusions and outlook

The results presented here illustrate the far-reaching consequences of mild local variation of one of the parameters (the temperature) governing reactivity in a two-dimensional model system. The main purpose of this contribution was to explore novel spatiotemporal policies for controlling reactions governed by coupling of (nonlinear) kinetics and diffusion. In this paper some of the recent work along these lines has been reviewed and new results from our ongoing effort have been presented. Progressing from simple spatiotemporal perturbations in one- or two-shot experiments, we investigated how the systems responds to subcritical excitations and their cooperative effects toward more complex approaches. Guiding or annihilating waves and the effects of local periodic forcing have been presented. Finally a strategy to improve surface reactivity has been explored.

Although the studied reaction system is quite simple, it is well suited as a model to test new approaches to control and influence nonlinear systems. Transfer of the principles outlined in this paper to “real” three-dimensional appropriately transparent catalyst beds might, at least in principle, be possible, but achieving improvements of the yield and/or selectivity on a large-scale production is not very likely. On the other hand, it is felt that much more may be learned from spatiotemporally resolved actuation in microchemical (e.g., “lab on a chip”) or biological (e.g., cellular) systems because of their inherent high complexity.

Acknowledgments

This work was partially supported by AFOSR (Dynamics and Control) and by a Humboldt Forschungspreis to I.G.K, as well as a Princeton PPL Fellowship to X. Li, and by a Marie Curie Individual Fellowship (A.G.P.) under Contract HPMFCT-2000-00685.

References

[1] B. Ogunnaike, W.H. Ray, Process Dynamics, Modeling and Control, Oxford Univ. Press, New York, 1994.
[2] V.K. Vanag, L.F. Yang, M. Dolnik, A.M. Zhabotinsky, I.R. Epstein, Nature 406 (2000) 389.
[3] J. Wolff, A.G. Papathanasiou, I.G. Kevrekidis, H.H. Rotermund, G. Ertl, Science 294 (2001) 134.
[4] J.R. Hahn, W. Ho, Phys. Rev. Lett. 87 (2001) 166102.
[5] J.K. Nørskov, Nature 414 (2001) 405.
[6] A.G. Papathanasiou, J. Wolff, I.G. Kevrekidis, H.H. Rotermund, G. Ertl, Chem. Phys. Lett. 358 (2002) 407–412.
[7] H.H. Rotermund, G. Haas, R.U. Franz, R.M. Tromp, G. Ertl, Science 270 (1995) 608.
[8] M. Feinberg, D. Terman, Arch. Rational Mech. Anal. 116 (1991) 35.
[9] M. Eiswirth, J. Bürger, P. Strasser, G. Ertl, J. Phys. Chem. 100 (1996) 19118.
[10] F. Schüth, B.E. Henry, L.D. Schmidt, Adv. Catal. 39 (1993) 51.
[11] K. Krischer, M. Eiswirth, G. Ertl, J. Chem. Phys. 96 (1992) 9161.
[12] T. Gritsch, D. Coulman, R.J. Behm, G. Ertl, Phys. Rev. Lett. 63 (1989) 1086.
[13] T. Gritsch, D. Coulman, R.J. Behm, G. Ertl, Appl. Phys. A 49 (1989) 403.
[14] R. Ducros, R.P. Merril, Surf. Sci. 55 (1976) 227.
[15] N. Freyer, M. Kiskinova, G. Pirug, H.P. Bonzel, Surf. Sci. 166 (1986) 206.
[16] J. Wolff, A.G. Papathanasiou, H.H. Rotermund, G. Ertl, M.A. Katsoulakis, X. Li, I.G. Kevrekidis, Phys. Rev. Lett., in press.
[17] J. Wolff, A.G. Papathanasiou, H.H. Rotermund, G. Ertl, M.A. Katsoulakis, X. Li, I.G. Kevrekidis, Phys. Rev. Lett. 90 (2003) 018302.